BAMS Article

The Polar Radiant Energy in the Far Infrared Experiment

A New Perspective on Polar Longwave Energy Exchanges

Tristan S. L'Ecuyer, Brian J. Drouin, James Anheuser, Meredith Grames, David S. Henderson, Xianglei Huang, Brian H. Kahn, Jennifer E. Kay, Boon H. Lim, Marian Mateling, Aronne Merrelli, Nathaniel B. Miller, Sharmila Padmanabhan, Colten Peterson, Nicole-Jeanne Schlegel, Mary L. White, and Yan Xie

ABSTRACT: Earth's climate is strongly influenced by energy deficits at the poles that emit more thermal energy than they receive from the sun. Energy exchanges between the surface and atmosphere influence the local environment while heat transport from lower latitudes drives midlatitude atmospheric and oceanic circulations. In the Arctic, in particular, local energy imbalances induce strong seasonality in surface–atmosphere heat exchanges and an acute sensitivity to forced climate variations. Despite these important local and global influences, the largest contributions to the polar atmospheric and surface energy budgets have not been fully characterized. The spectral variation of far-infrared radiation that makes up 60% of polar thermal emission has never been systematically measured impeding progress toward consensus in predicted rates of Arctic warming, sea ice decline, and ice sheet melt. Enabled by recent advances in sensor miniaturization and CubeSat technology, the Polar Radiant Energy in the Far Infrared Experiment (PREFIRE) mission will document, for the first time, the spectral, spatial, and temporal variations of polar far-infrared emission. Selected under NASA's Earth Ventures Instrument (EVI) program, PREFIRE will utilize new lightweight, low-power, ambient temperature detectors capable of measuring at wavelengths up to 50 μm to quantify Earth's far-infrared spectrum. Estimates of spectral surface emissivity, water vapor, cloud properties, and the atmospheric greenhouse effect derived from these measurements offer the potential to advance our understanding of the factors that modulate thermal fluxes in the cold, dry conditions characteristic of the polar regions.

KEYWORDS: Antarctica; Arctic; Climate change; Energy budget/balance; Radiation budgets; Satellite observations

https://doi.org/10.1175/BAMS-D-20-0155.1
Corresponding author: Tristan S. L'Ecuyer, tristan@aos.wisc.edu
In final form 23 February 2021

AFFILIATIONS: L'Ecuyer—University of Wisconsin–Madison, and Cooperative Institute for Meteorological Satellite Studies, Madison, Wisconsin; **Drouin, Kahn, Lim, Padmanabhan, Schlegel, and White**—Jet Propulsion Laboratory, California Institute of Technology, Pasadena, California; **Anheuser, Grames, and Mateling**—University of Wisconsin–Madison, Madison, Wisconsin; **Henderson, Merrelli, and Miller**—Space Science and Engineering Center, Madison, Wisconsin; **Huang, Peterson, and Xie**—University of Michigan, Ann Arbor, Michigan; **Kay**—University of Colorado Boulder, Boulder, Colorado

The poles play an essential role in regulating Earth's climate. The steep angle at which sunlight illuminates the higher latitudes coupled with reflective snow- and ice-covered surfaces and the long period of darkness during local winter significantly reduces the solar input into the poles. However, these regions emit thermal radiation throughout the year resulting in substantial net energy deficits on annual time scales. The National Aeronautics and Space Administration (NASA) Energy and Water cycle Study (NEWS) reconstruction of the polar energy budgets in the first decade of the twenty-first century suggests that the Arctic emits 2.4 times as much energy as it receives from the sun. This ratio increases to 2.8 over the brighter, colder Antarctic ice sheet (L'Ecuyer et al. 2015, their Table 4). In the absence of compensating processes, the resulting rate of energy loss, that exceeds a petawatt (10^{15} watts) at each pole, would cause the poles to cool rapidly even relative to current conditions. Neglecting the effects of anthropogenic climate change, equilibrium is restored by heat transported from lower latitudes primarily by atmospheric circulations and midlatitude weather systems. As such, the poles can be thought of as Earth's thermostats, balancing the excess solar energy received in the tropics through their radiative losses to space.

Energy imbalances in the polar regions have consequences both locally and globally. A key component of these imbalances, longwave emission, has been shown to impact sea ice cover, ice sheet melt, and, by extension, Arctic temperatures (Francis et al. 2005; Schweiger et al. 2008; Bennartz et al. 2013; Van Tricht et al. 2016; Kapsch et al. 2016; Johansson et al. 2017). Beyond these local effects, polar energy imbalances influence global sea level through glacial melt (Slater et al. 2020), midlatitude weather (Francis and Vavrus 2012; Vihma 2014), and, ultimately, global temperatures (Budyko 1969). Accurate estimates of thermal flux exchanges between the surface, atmosphere, and space at the poles and the factors that modulate them are, therefore, essential for modeling polar and global climate.

The need for comprehensive observations of thermal flux exchanges in the Arctic is particularly acute since this region is changing more rapidly than anywhere else on Earth with considerable societal implications. Predicting the Arctic and global responses to anthropogenic climate change requires quantitative understanding of Arctic feedbacks that are intimately coupled to longwave fluxes. However, comparing estimates of Arctic surface and atmospheric longwave fluxes from various sources reveals large uncertainties in both surface emission and downwelling longwave radiation (DLR). Figure 1 compares decade mean annual cycles of surface longwave fluxes in the Arctic and Antarctica for the first decade of the twenty-first century from three commonly used sources: observations, reanalyses, and models from the fifth Coupled Model Intercomparison Project (CMIP5). The period analyzed (2000–09) maximizes the availability of the various datasets while reducing the effects of interannual variability to yield a snapshot of the current state of knowledge of these fluxes. Estimates of Arctic surface emission and DLR, a proxy for the atmospheric greenhouse effect (AGHE), vary by 35–70 W m^{-2} between sources with the largest uncertainties in the winter months. These discrepancies have significant implications for the longer-term evolution of the polar climates.

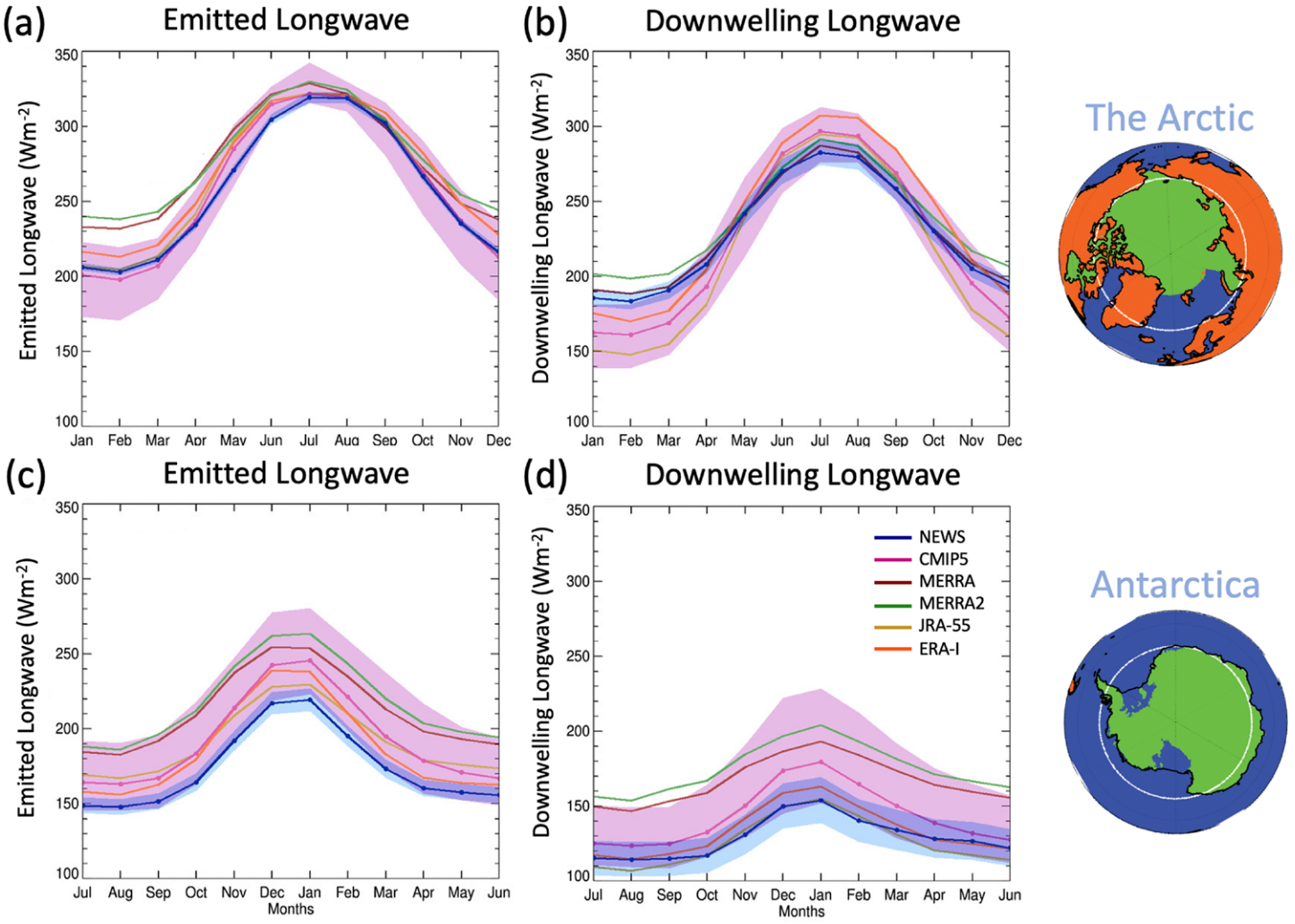

Fig. 1. (a),(b) Arctic and (c),(d) Antarctic surface thermal flux estimates from observations, reanalyses, and CMIP5 models. The blue lines depict the NEWS polar energy budget reconstructions that imposed energy and water balance constraints on independent satellite-based flux estimates (L'Ecuyer et al. 2015). The pink and blue swaths correspond to the range across CMIP5 models and estimated uncertainties in the NEWS analysis, respectively. The definitions of the Arctic and Antarctica are presented as the green shaded regions on the right consistent with the NEWS analyses. Note: Antarctic annual cycles are offset by 6 months relative to the Arctic to facilitate direct comparisons.

When integrated over the year, for example, net longwave radiation incident on the Arctic surface, defined as the difference between DLR and surface emission, ranges from –24 to –54 W m^{-2} across the sources shown. This translates to a 0.3 PW (or 25%) uncertainty in implied heat transport from lower latitudes. Antarctica is colder and drier than the Arctic leading to reduced surface emission and DLR. This also inhibits phase changes at the surface reducing the amplitude of the annual cycle of thermal fluxes. However, despite these more stable boundary conditions, the spreads in estimated surface emission and DLR among the CMIP5 models is larger than in the Arctic reaching 70 and 80 W m^{-2}, respectively. Unlike the Northern Hemisphere, the largest spread in Antarctic flux estimates occur during the Southern Hemisphere summer months.

These uncertainties are at least as large as those in their shortwave counterparts (L'Ecuyer et al. 2015) and directly contribute to errors in surface energy balance and, in turn, surface warming and melt processes (Gardner 2010). Our ability to narrow this range in polar longwave flux estimates and the resulting spread in predicted local processes and global climate is, however, impeded by a critical gap in global observations of a significant fraction of Earth's emission spectrum.

The far-infrared observation gap

At terrestrial temperatures, more than 99% of thermal emission occurs at wavelengths between 4 and 100 μm. Given the central role thermal fluxes play in the climate and their strong sensitivity to atmospheric composition and clouds, radiation at midinfrared (MIR) wavelengths (4–15 μm) has been extensively measured from the ground, aircraft, and throughout the satellite era (Ackerman et al. 2019). This is not the case, however, for radiation at wavelengths longer than 15 μm, termed the far-infrared (FIR), that account for about half of Earth's outgoing longwave radiation (Harries et al. 2008).

The paucity of systematic measurements of Earth's FIR emission spectrum stems, in part, from the higher cost required to achieve similar sensitivities to current MIR measurements. Until recently, resolving complete FIR spectra has required either long integration times that translate into large footprints and preclude capturing localized spectra from low-Earth orbit or cryogenically cooled detectors. The Infrared Interferometer Spectrometer (IRIS)-B and IRIS-D instruments flown on *Nimbus-3* and *Nimbus-4* in 1969 and 1970 provided tantalizing glimpses at Earth's long wavelength thermal emission spectrum from space (up to 25 μm); however, the integration time required to capture these spectra poses significant hurdles for localized geophysical parameter retrievals (Conrath et al. 1970; Hanel et al. 1970, 1971; Prabhakara et al. 1974, 1976, 1988). Despite significant advances in sensor technology, spectroscopy, and our understanding of the role of far-infrared radiation in climate, only a few short-lived satellite-based experiments have measured emitted spectra at wavelengths longer than 15 μm, the last taking place more than four decades ago (Spankuch and Dohler 1985). Subsequent FIR measurements have been limited to broadband measurements [e.g., *Earth Radiation Budget Satellite* (*ERBS*), Earth Radiation Budget Experiment (ERBE), Scanner for Radiation Budget (ScaRaB), Geostationary Earth Radiation Budget (GERB), and Clouds and the Earth's Radiant Energy System (CERES)] or spectra from ground-based and airborne campaigns precluding any large-scale survey of the character of Earth's far-infrared emission (Palchetti et al. 2020).

The significance of this FIR observing gap is highlighted in Fig. 2a that presents Earth's annual mean emission spectrum in 2019 obtained by extrapolating MIR Atmospheric Infrared Sounder (AIRS) measurements to longer wavelengths (Huang et al. 2014b). The region left of 667 cm^{-1} (15 μm) accounts for nearly half (49.1%) of global emission. In Antarctica in winter (blue curve), the fraction of emission in the FIR exceeds 60%. Figure 2b suggests that FIR radiation makes up a significant component (between 40% and 65%) of thermal emission everywhere on the globe. The largest fractions occur in colder, drier regions such as the Antarctic and Greenland ice sheets, high alpine regions, and areas of persistent high cloud cover in the deep tropics.

There are numerous tangible benefits to extending existing spectral longwave emission measurements into the FIR. At these longer wavelengths, radiation exhibits distinct sensitivities to surface conditions, thin ice clouds, and tenuous water vapor filaments that may offer new insights into these less observed components of the climate system. For example, sea ice and ocean have lower emissivities in the FIR relative to vegetated surfaces and the emissivity of snow-covered surfaces exhibits depends strongly on snow grain size (see Fig. 3 and discussion below). The sensitivity of FIR radiation to low concentrations of water vapor at low temperatures also makes FIR spectra useful for retrieving moisture in the polar regions as well as the upper troposphere and lower stratosphere (UTLS) (Turner and Mlawer 2010; Merrelli and Turner 2012; Shahabadi and Huang 2014; Palchetti et al. 2015). Furthermore, the indices of refraction of liquid and ice exhibit distinct spectral variations across the MIR and FIR, augmenting existing MIR techniques for cloud phase detection (Rathke et al. 2002; Turner et al. 2003; Maestri et al. 2019b; Di Natale et al. 2020). Furthermore, small ice particles are comparable in size to FIR wavelengths enhancing FIR sensitivity to ice cloud

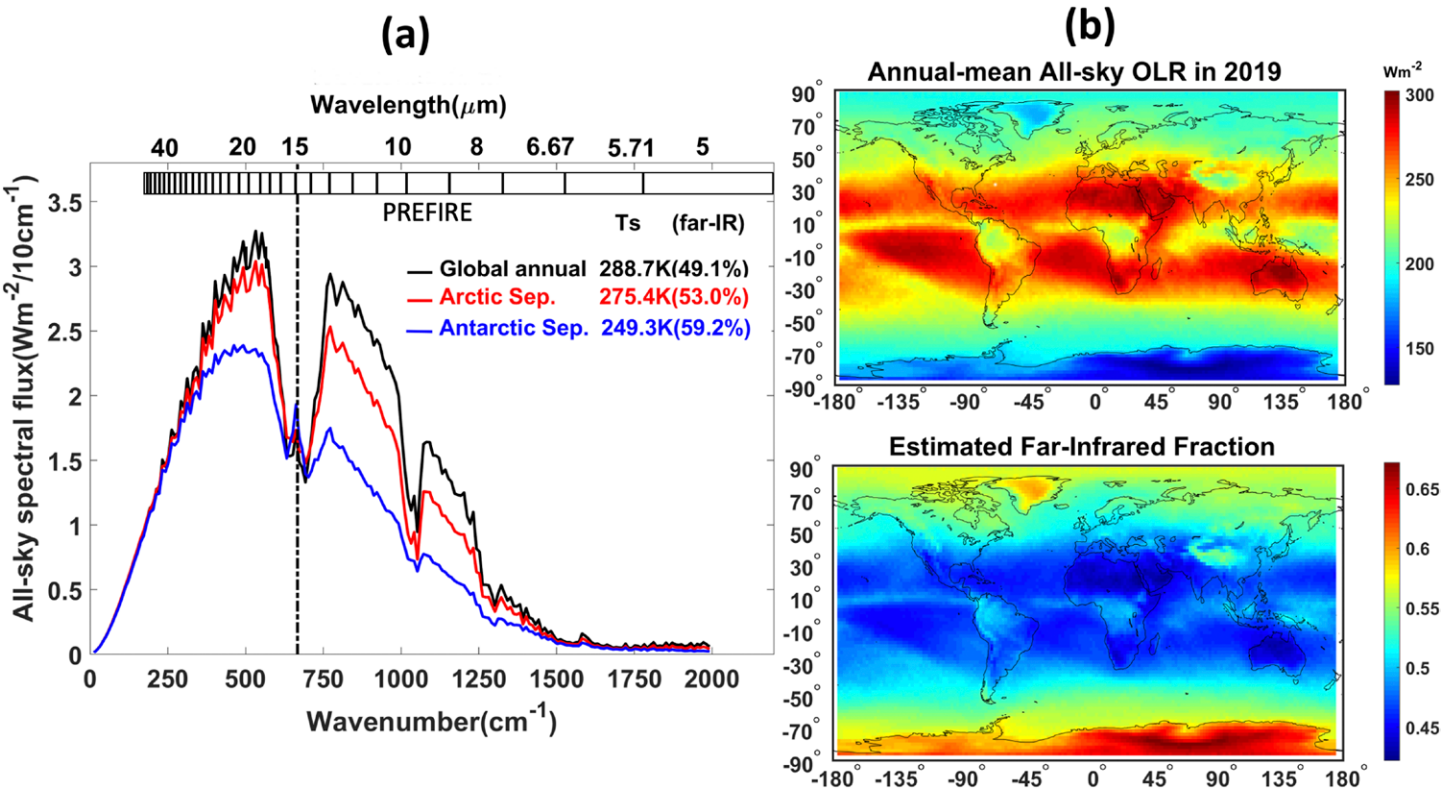

Fig. 2. (a) Global, annual mean all-sky longwave spectral flux derived from AIRS measurements from 2019 (black) and polar emission spectra from the Arctic (red) and Antarctica (blue) in September 2019. The spectral flux is shown for every 10 cm^{-1} interval from 0 to 2,000 cm^{-1} (details can be found in Huang et al. 2014b). Corresponding mean surface temperatures are also indicated in the legend. Current multi- and hyperspectral satellite measurements observe MIR wavelengths to the right of the vertical dash–dotted line. PREFIRE will measure the full range of wavelengths indicated by the striped bar across the top of the figure (see Fig. 7 for precise locations of the PREFIRE spectral bands). (b) Annual-mean all-sky OLR in 2019 derived from the (top) collocated AIRS and CERES observations and (bottom) the fraction of this estimated OLR contributed by FIR wavelengths.

particle size offering potential for improving global cloud microphysical property retrievals (Yang et al. 2005, 2003; Baran 2007; Libois and Blanchet 2017; Saito et al. 2020).

Since surface emission, liquid and ice clouds, and atmospheric water vapor each exhibit distinct spectral signatures, FIR spectra carry the fingerprints of variations in each constituent providing insights into their respective feedbacks in the climate system (Huang et al. 2014a; Pan and Huang 2018). Huang et al. (2019), for example, demonstrate that FIR signatures can be used to isolate distinct cloud feedback mechanisms. They show that, while broadband longwave cloud feedbacks derived from the prescribed sea surface temperature simulations and long-term 2 × CO_2 simulations are similar, their partitioning between the FIR and MIR can be considerably different due to different cloud profile responses.

Implications of incomplete knowledge

FIR radiation plays a particularly important role in shaping polar climate. Cold polar surfaces emit the majority of their energy in the FIR where snow- and ice-covered surfaces are predicted to exhibit strong emissivity variations (Huang et al. 2016). Dry polar atmospheres are typically more transparent to FIR radiation than those at lower latitudes allowing more of this surface emission to reach space in clear skies. However, water vapor effectively absorbs far-infrared radiation so outgoing longwave radiation (OLR) and DLR are very sensitive to both water vapor concentration and its spectroscopic properties in the FIR (Clough et al. 1992; Turner and Mlawer 2010). In cloudy skies, ice particle scattering becomes increasingly important in the FIR increasing the sensitivity of OLR to ice crystal habit and particle

size distribution (Maestri and Rizzi 2003; Baran 2007; Yang et al. 2013; Kuo et al. 2018; Chen 2020). Thus, spectral variations in surface emissivity, water vapor absorption, and ice cloud optical properties across the FIR play a key role in defining polar energy imbalances but significant uncertainties remain in each owing to the limited availability of measured far-infrared spectra to constrain them (Huang et al. 2018; Mlawer et al. 2019; Bantges et al. 2020).

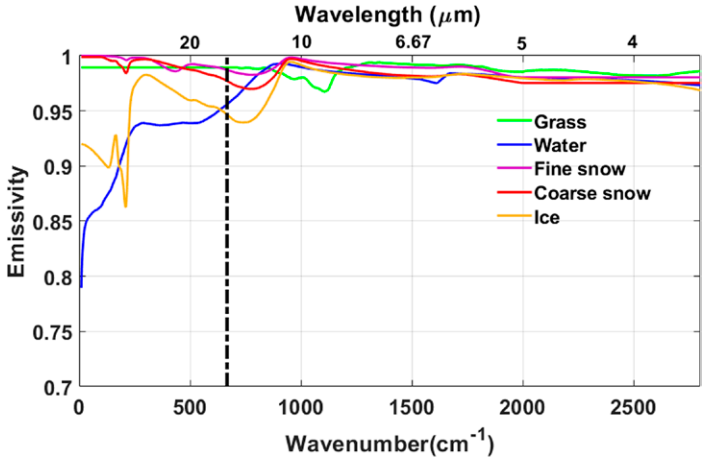

Fig. 3. Simulated mid- and far-infrared emissivity spectra for selected surface types found in the polar regions based on Huang et al. (2016). The FIR emissivity of grass is extrapolated from the nearest available MIR measurement. The FIR emissivities of the remaining surface types are based on first-principal calculations while MIR emissivities are validated against observations.

Incomplete knowledge of the radiative properties of the surface and atmospheric constituents in the FIR has important consequences for accurately modeling several aspects of the climate system. Turner et al. (2012) demonstrate that water vapor continuum absorption in the FIR could lead to uncertainty in the vertical distribution of thermal fluxes in the atmosphere subsequently influencing temperature, water vapor, and high cloud amount (both globally and poleward of 60°) in simulations using the Community Earth System Model (CESM; v1.0). FIR surface emissivities provide another example. Due to sparse observational constraints on spectral FIR emissivity, current climate models either assume the surface emissivity of an ideal blackbody (i.e., unit emissivity) or extrapolate emissivities from atmospheric window channels in the MIR across the FIR. However, theoretical calculations, laboratory measurements, and limited aircraft observations suggest that common polar surfaces exhibit significant and distinct variations in spectral emissivity across the FIR (Huang et al. 2016; Bellisario et al. 2017; Murray et al. 2020). The simulated emissivity spectra presented in Fig. 3, for example, highlight significant differences in the FIR emissivities of snow, ice, and liquid water that can exceed 10% at some wavelengths. Sensitivity studies using the *CloudSat* radiative fluxes and heating rates product [2B-FLXHR-lidar, described in Henderson et al. (2013)] suggest that ignoring these spectral variations introduces annual mean biases of at least 10 W m^{-2} in surface emission across the entire Arctic.

Biases of this magnitude can have substantial implications for modeling both ice surface processes and the Arctic climate as a whole. Sensitivity studies using a state-of-the-art ice sheet dynamics and surface mass balance model, for example, show that the increase in net surface radiation that results from realistic emissivity assumptions enhances both meltwater runoff and ice temperatures (Gardner 2010). When further coupled to atmospheric and ocean models as part of a complete Earth system model, the effects of spectral surface emissivity errors may propagate to influence other aspects of polar climate. For example, incorporating the theoretical spectral surface emissivity models shown in Fig. 3 into the NCAR Community Earth System Model version 1 (CESM1) and the DOE Energy Exascale Earth System Model (E3SM) leads to an increase of global annual mean surface air temperature of ~0.2 K for the fully coupled CESM1 and E3SM simulations (Huang et al. 2018; Kuo et al. 2018; Chen 2020). Mean surface air temperature increases at high latitudes are more than 3 times as large and are accompanied by significant reductions in sea ice fraction, as shown in Fig. 4.

Model responses to surface emissivity errors are, however, not uniform across the Arctic. Annual mean surface temperatures in the Greenland and Barents Seas, for example, increase by more than 2.5 K reducing annual mean sea ice cover by more than 15% in these regions.

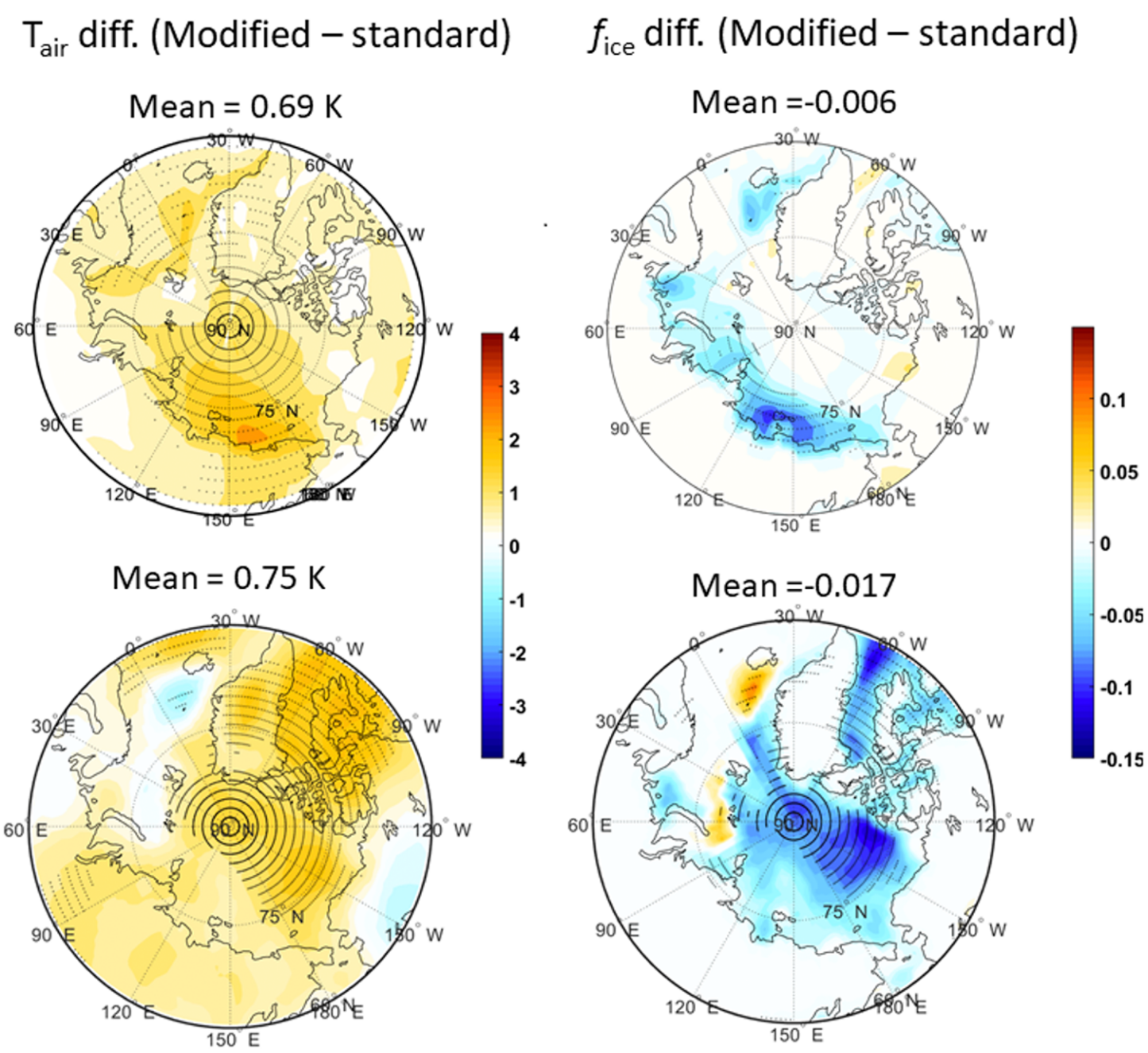

Fig. 4. Difference in Arctic (left) surface air temperature and (right) sea ice fraction climatology from incorporating realistic surface spectral emissivity into (top) the NCAR CESM1 and (bottom) the DOE E3SM v1. Both are fully coupled present-day simulations. Dots on the plots denote statistically significant differences at the 5% significance level (Huang et al. 2018; Chen 2020).

For both models, spectral variations in FIR surface emissivity effectively increase the radiation absorbed at the surface by 2%–5%, roughly equivalent to half the magnitude of the forcing from doubling atmospheric CO_2 concentrations. Though they arise through different mechanisms, the effects of spectral variations in surface emissivity are similar to increasing the atmospheric greenhouse effect: when they are accumulated over a decade in the GCM, the additional accumulated surface radiation reduces sea ice extent, increases surface temperature, and even increases precipitation. However, the magnitude and distribution of these responses depends critically on model physics. The spatial pattern, seasonality, and magnitude of these effects are all influenced by clouds, surface state, and parameterized physical processes (e.g., Sledd and L'Ecuyer 2019). Better observational constraints on FIR emissivity and the atmospheric greenhouse effect would enable systematic comparisons

across multiple models to more thoroughly assess their impacts on Arctic warming, ice melt rates, and global climate.

Filling the gap

Recognizing the value of FIR observations, both NASA and the European Space Agency (ESA) recently selected complementary satellite missions dedicated to mapping Earth's far-infrared emission globally. Palchetti et al. (2020) describe ESA's Far-infrared Outgoing Radiation Understanding and Monitoring (FORUM) mission that will launch in 2026 to benchmark the far-infrared fingerprints of global climate forcings in high-spectral-resolution far-infrared observations. This paper describes a complementary, low-cost, rapid development NASA mission, Polar Radiant Energy in the Far Infrared Experiment (PREFIRE), that will employ two CubeSats to measure the far-infrared signatures of the surface and atmospheric processes that influence polar climate. PREFIRE documents variability in moderate-spectral-resolution far-infrared spectra on subdaily to seasonal time scales to more completely characterize longwave fluxes at the poles and improve their representation in both local and global models.

The PREFIRE mission combines recent advances in ambient temperature detector and optical spectrometer technology with rapidly evolving CubeSat capabilities to map spectral emission from 5 to 54 μm. This range covers more than 95% of Earth's thermal emission to space. These observations form the basis for quantifying variations in spectral surface emissivity and atmospheric greenhouse effect associated with changing surface conditions, variations in atmospheric moisture content, and the presence of clouds at both poles.

Collecting spectra in all seasons, PREFIRE's CubeSats will provide a census of the temporal and spatial character of FIR radiation in polar regions and provide pathways for using these observations to advance polar climate prediction. The relatively transparent polar atmospheres allow snow and ice FIR emissivity spectra to be quantified on hourly to seasonal time scales provided integrated water vapor is low and cloudy scenes can be accurately identified and screened. Algorithms leveraging the sensitivity of MIR and FIR radiances to temperature, water vapor, and clouds will characterize the response of the atmospheric greenhouse effect to both transient and seasonal variations in water vapor, cloud cover, and local surface processes. When coupled to models of ice sheet surface energy budget dynamics, the influence of surface emissivity and AGHE variations on modeled ice sheet temperature, mass balance, and thermodynamic processes can be assessed on hourly to weekly scales. Finally, time-varying estimates of spectral surface emissivity and top of atmosphere FIR spectra offer a pathway to improving surface emission in global models and identifying specific sources of error through their FIR fingerprints.

The PREFIRE mission

Thoroughly documenting polar emission requires observations of spectral radiances across the MIR and FIR over the range of surfaces and atmospheric conditions encountered at both poles throughout the year. In addition, quantifying the spectral signatures of rapid surface processes such as melt events or atmospheric variations associated with changing cloud cover necessitates occasional revisits of some locations at time intervals of a few hours. PREFIRE satisfies both of these requirements for a relatively low cost by employing two CubeSat's in asynchronous high-inclination orbits each carrying an identical lightweight, low-power spectrometer. The mission concept is illustrated in Fig. 5. Two spacecraft continuously map emission spectra over most of Earth in high-inclination orbits (Fig. 5, center). Each satellite carries a Thermal Infrared Spectrometer (TIRS) that collects 64-channel spectra spanning wavelengths up to 54 μm in each of eight cross-track fields of view every 0.7 s.

As technological advances promote increased use of Smallsats and CubeSats like PREFIRE (Stephens et al. 2020), it is fair to ask whether such low-cost platforms with limited lifetimes

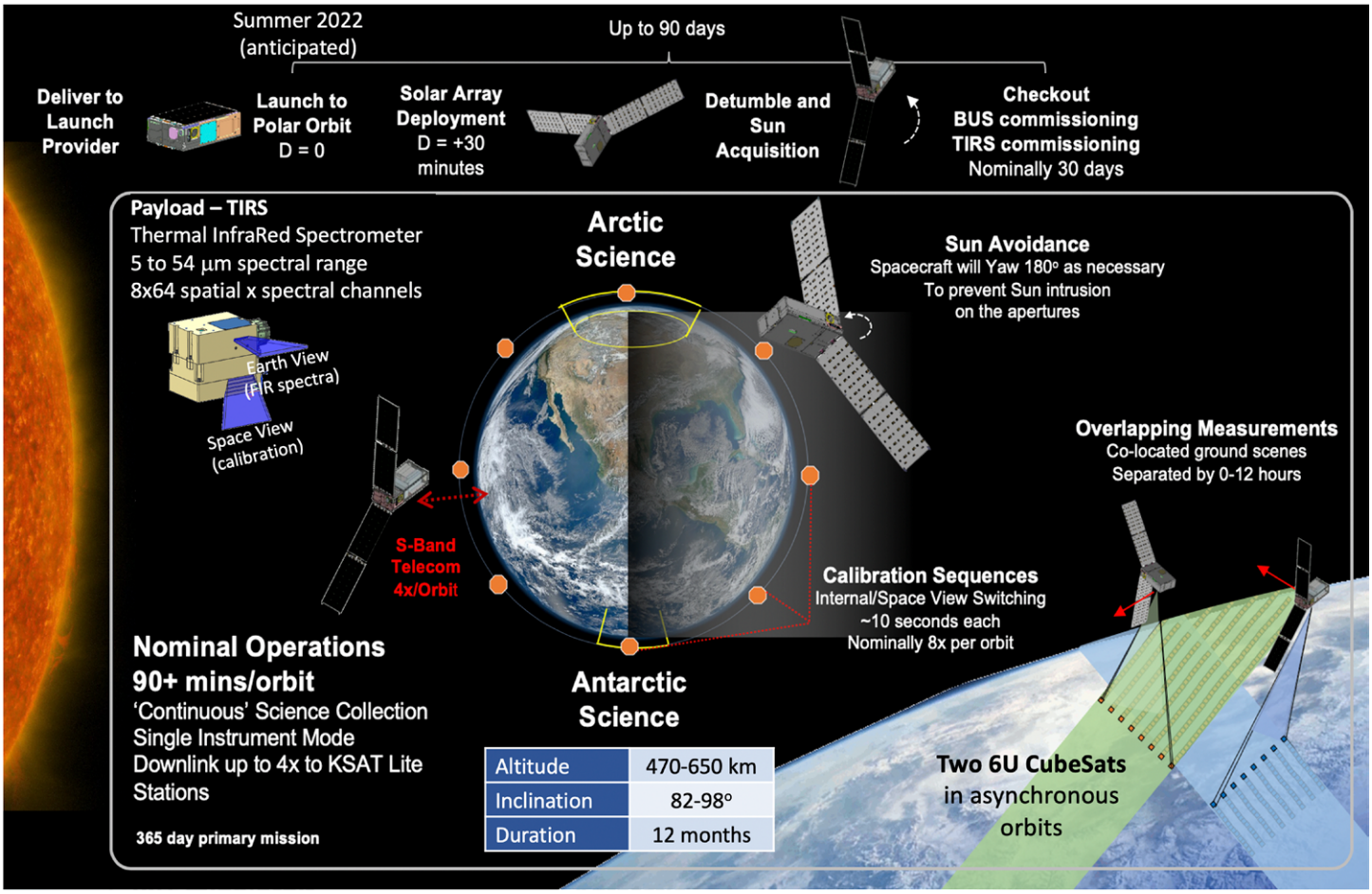

Fig. 5. The PREFIRE mission concept. Two CubeSats flying in distinct polar low-Earth orbits map FIR spectra at both poles. Orbit intersections at intervals of 1–12 h reveal the spectral signatures of surface processes and rapid atmospheric variations. Additional information can be obtained from the PREFIRE website: https://prefire.ssec.wisc.edu.

will offer similar coverage in time and space as present-day NASA flagship missions like *Aqua*. Each TIRS can make over 200 million spatially and spectrally resolved observations of Earth's polar radiant thermal energy in a year but to what extent do these observations span the range of column water vapor (CWV), surface temperature T_{sfc}, and surface conditions (land, ocean, sea ice, glacier ice, snow) encountered at the poles? To address this question, Kahn et al. (2020) compared the subset of AIRS and Advanced Microwave Sounding Unit (AMSU) observations corresponding to 93°, 98°, and 103° inclination TIRS orbits, to full-swath AIRS/AMSU climatologies. The analysis concludes that each year of TIRS data samples 74%–82% of a 2-yr full-swath AIRS/AMSU climatology. The sampling rates for the Arctic (60°–90°N) and Antarctic (70°–90°S) individually drop to 62%–75% and 47%–71%, respectively. This demonstrates the value of pooling data from both poles to fill out the complete spectrum of polar weather states ranging from the ice-free ocean prevalent in the Arctic in September to the cold, dry regions above the Antarctic and Greenland ice sheets in winter.

The ability to identify and characterize the FIR spectral signatures of rapid processes like sudden melt events is realized by simultaneously operating two CubeSats with identical TIRS instruments. Time-differenced spectra obtained from the orbit intersections of these CubeSats (illustrated in the lower right of Fig. 5) reveal the spectral fingerprints of specific surface and atmospheric processes diagnosed using ancillary observations or reanalyses. Over the course of several months, PREFIRE's CubeSats will sequentially pass over melt, freeze, and fresh snow events occurring on both sea ice and ice sheets. There is a high likelihood that such intersections will also sample atmospheric variability associated with changing cloud cover

or water vapor intrusions to reveal the spectral signatures of their influence on FIR emission and AGHE. Any combination of equatorial crossing times is suitable for the purpose of observing these polar processes since the resulting orbit intersections result in a range of time differences Δt spanning one to several hours, consistent with the time scales of short-term melt events and transient cloud changes. While the specific orbits of the PREFIRE CubeSats will not be known until a specific launch is selected (nominally in late 2022), it is anticipated that they will fly in asynchronous orbits in an altitude range of 450–540 km at inclinations between 70° and 98°.

The Thermal Infrared Spectrometer

Each PREFIRE CubeSat will carry its own TIRS, a push broom spectrometer with 64 channels that measures mid- and far-infrared radiation from 5 to 54 μm at 0.86-μm resolution. The dimensions and a rough schematic of the TIRS are shown in Fig. 6. TIRS continuously records eight cross-track pixels with a ground spacing of approximately 7 km. To meet the mass, power, and cost constraints imposed by a CubeSat platform, an uncooled focal plane is essential. TIRS is thermally isolated from the spacecraft and regulated through controlled dissipation of its steady-state power. Eight or more times per orbit, TIRS is calibrated by rotating a calibration mirror to provide space and internal calibration views (Fig. 5). Internal calibration includes a radiometric measure of all light (thermopile detectors are sensitive to 0.3–200 μm) using the zeroth-order reflection off the grating. Additional calibration will be provided via in-flight comparisons with other satellites and ground data.

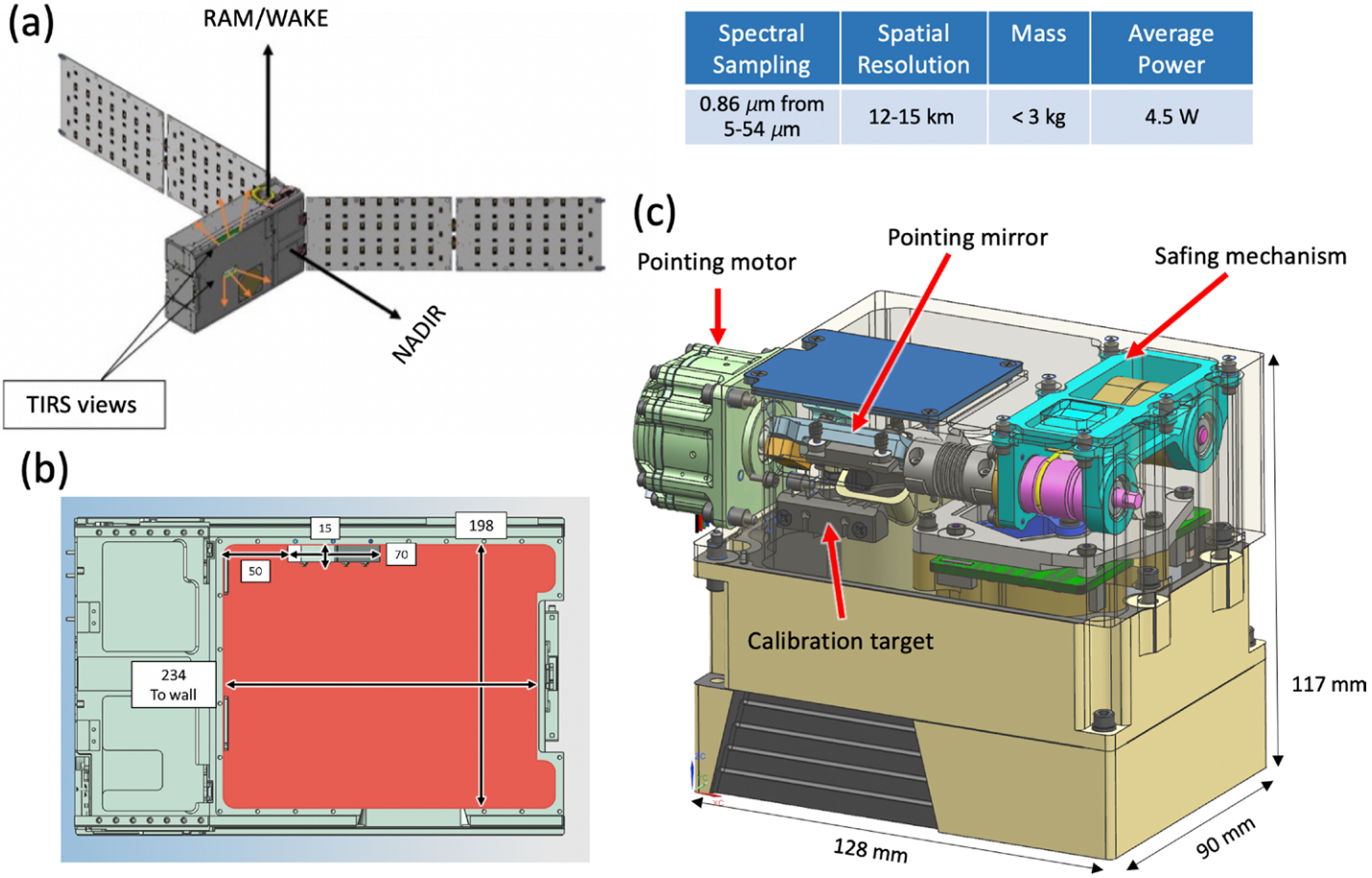

Fig. 6. (a) Approximate form of the PREFIRE 6U CubeSat and (b) corresponding interior layout and dimensions. The total dimensions of each CubeSat are 300 mm long, 200 mm wide, and 100 mm deep. (c) The TIRS instrument will occupy just over half of this space.

TIRS effective field of view (EFOV) will be comparable to that of CERES or AIRS, between 12 and 15 km depending on its final orbit altitude. Prior work has demonstrated that this is sufficient to adequately screen thin clouds (Kahn et al. 2014) and capture bulk variations in surface emissivity (e.g., Hulley et al. 2009; Zhou et al. 2008). Subpixel variability will be assessed using algorithms trained on high-resolution imagery and tested using simultaneous overpasses of current shortwave and MIR imagers. The expected radiometric performance of TIRS is better than 1.5 K (at 300 K) for all individual MIR and FIR channels from 5 to 54 μm.

Characterizing polar thermal fluxes and their drivers

PREFIRE's scientific objectives of documenting the spectral characteristics of Earth's emission and greenhouse effect and understanding the factors that modulate them are supported by a suite of spectral radiative property and geophysical parameter retrievals. Calibrated, geolocated, 1-μm TIRS spectra, provide a census of the varying spectral signatures of emitted thermal radiation across the wide range of temperature, humidity, surface conditions, and cloud cover encountered over the Arctic and Antarctic annual cycles. Figure 7 illustrates a synthetic TIRS spectrum derived from collocated Airborne Research Interferometer Evaluation System (ARIES) and Tropospheric Airborne Fourier Transform Spectrometer (TAFTS) observations by simulating the effects of the atmosphere between the aircraft and TOA. Comparing the observed and simulated spectra at flight level and TOA highlights the strong impact of tenuous upper troposphere on FIR radiances and illustrates the relatively coarse TIRS resolution relative to an airborne spectrometer. These radiance spectra will then be converted to narrowband fluxes and a longwave broadband flux using established methods (Huang et al. 2008, 2010; Chen et al. 2013; Huang et al. 2014b). The approach relies on anisotropic distribution

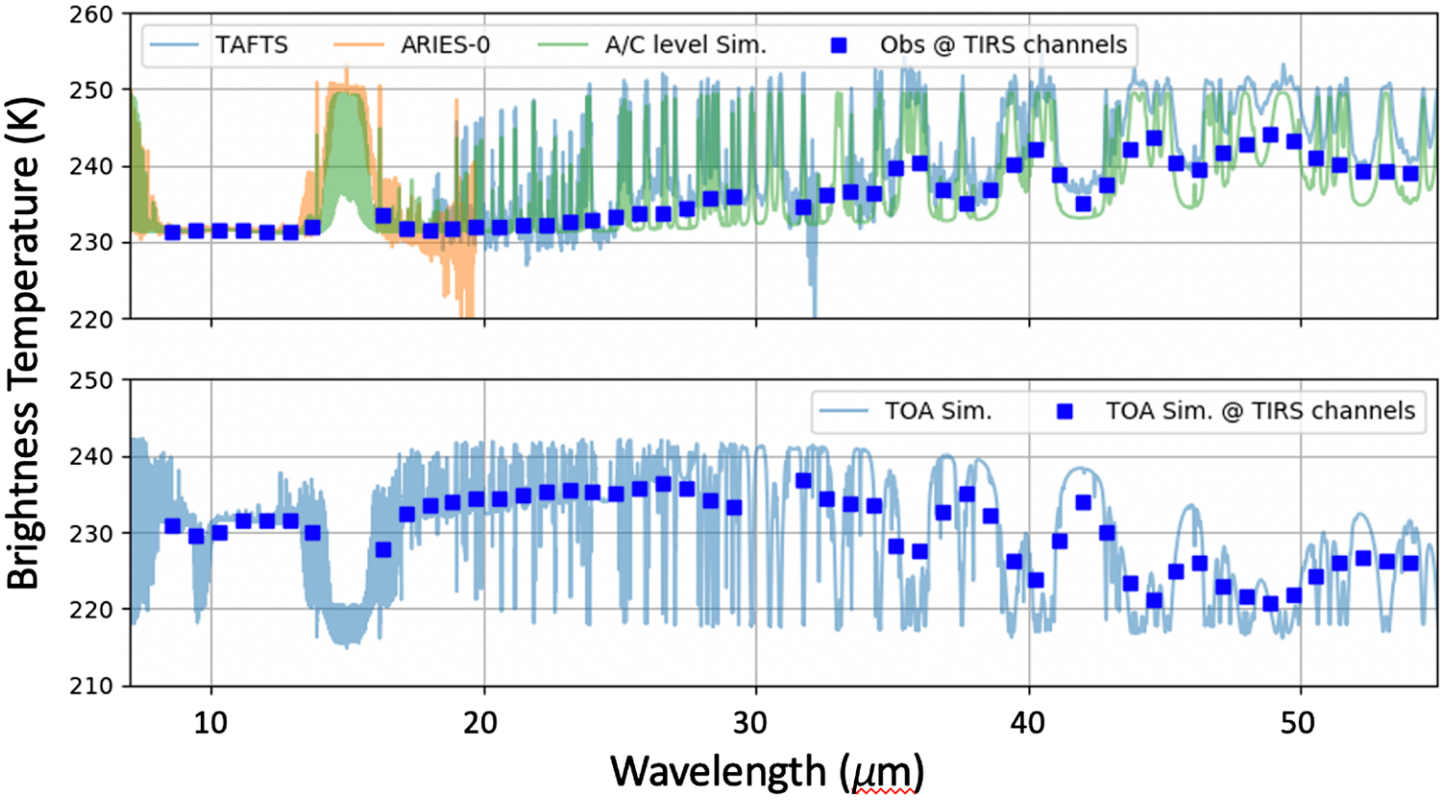

Fig. 7. (top) A MIR and FIR spectrum derived from collocated Airborne Research Interferometer Evaluation System (ARIES) and Tropospheric Airborne Fourier Transform Spectrometer (TAFTS) measurements during a low altitude flight over Greenland (Bellisario et al. 2017). (bottom) A simulated top of atmosphere spectrum for the same conditions. Radiances averaged over the anticipated spectral responses of the TIRS channels are plotted as blue boxes at the central wavelength of each channel.

models constructed for each predefined scene type. Application to AIRS radiances results in agreement to within 1%–2% of CERES OLR at the footprint level (Huang et al. 2008, 2010). Similar performance is expected for PREFIRE fluxes given the trade-off between the reduced spectral sampling but increased spectral coverage of the TIRS.

To aid in understanding the factors that modulate polar longwave fluxes, a suite of geophysical parameters will also be derived from TIRS radiances. Table 1 summarizes these parameters, their anticipated accuracy, and preliminary plans for evaluating them. Scene characterization is an essential first step to retrieving atmospheric and surface properties.

Table 1. Anticipated PREFIRE data products. All data will be produced at the PREFIRE Science Data Processing System (SDPS) housed within the Space Science and Engineering Center (SSEC) at the University of Wisconsin–Madison.

Variable	Spectral range (sampling)	Anticipated accuracy	Product name
Geolocated radiance	5–54 μm (~1 μm)	1.5 K NEdT (at 300 K)	1B-RAD
Spectral fluxes	5–54 μm (~1 μm)	3% accuracy (10 W m^2 for total OLR; 4 W m^2 for FIR)	2B-FLX
Cloud mask	—	10% miss/false detection rate	2B-MSK
Surface temperature	—	2 K	2B-SFC
Spectral surface emissivity	5–30 μm (~5 μm)	1%	2B-SFC
Column water vapor (CWV)	—	10% for CWV > 0.1 mm	2B-ATM
Atmospheric temperature	—	2 K	2B-ATM
Cloud phase and properties (experimental)	—	TBD	2B-CLD

The PREFIRE cloud mask will build on the long heritage of cloud detection from satellite imagers from the Advanced Very High Resolution Radiometer to the Visible Infrared Imaging Radiometer Suite (VIIRS) (Rossow and Schiffer 1991; Ackerman et al. 1998, 2019). Similar approaches leveraging infrared split-window differences (e.g., Inoue 1985; Heidinger and Pavolonis 2009), CO_2-slicing channels (Menzel et al. 2008), and 6.3-μm water vapor channels within a physically grounded estimation framework have been successfully adapted to infrared sounders with footprints similar to TIRS such as AIRS (Kahn et al. 2014). Simulated clear-sky radiances consistent with ancillary T_{sfc} and atmospheric soundings from reanalyses are subtracted from observed TIRS radiances. Differences larger than instrument noise and scene-dependent uncertainty in surface and atmospheric profiles are indicative of clouds. The sensitivity of the cloud mask is, therefore, determined by three factors: instrument noise, the accuracy of ancillary datasets, and the sensitivity of the TIRS radiances to cloud. Despite having coarser spectral sampling than AIRS, the sensitivity of the TIRS FIR channels to clouds and atmospheric water vapor should allow very thin clouds to be identified. Given its central role in subsequent clear-sky and cloudy-sky algorithms, assessing the accuracy of the PREFIRE cloud mask will be a focus of both prelaunch sensitivity studies and postlaunch validation activities.

For the subset of scenes determined to be cloud free with the highest confidence, TIRS MIR and FIR radiances provide complementary information for simultaneously inferring CWV, surface temperature, and surface emissivity using variational techniques that have strong heritage in the atmospheric sounding community. Figure 8 illustrates the physical basis for this algorithm. Simulated clear-sky spectra and selected weighting functions for Summit Station on the Greenland ice sheet (left) and the Greenland Sea (right) are shown, derived from the fifth-generation European Centre for Medium-Range Weather Forecasts (ECMWF) reanalyses (ERA5). Atmospheric window channels (e.g., 11 μm) are well suited

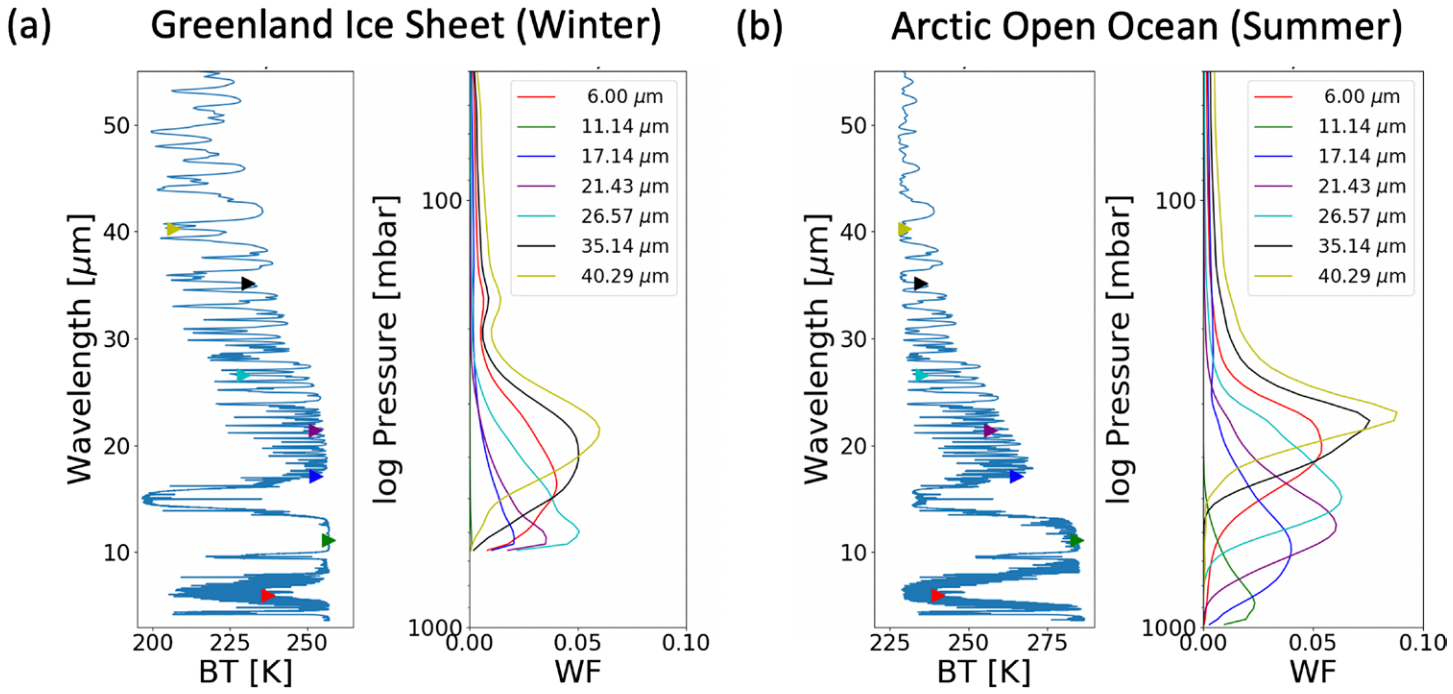

Fig. 8. Simulated clear-sky emission spectra and corresponding weighting functions from select ERA5 grid boxes located (a) on the Greenland ice sheet on 7 Jan 2016 and (b) in the Greenland Sea on 3 Jul 2016. The seven selected TIRS channels, corresponding to adjacent weighting functions, are represented by triangles overlying the high-resolution emission spectra.

for characterizing T_{sfc}, particularly in relatively dry polar climates (Key and Haefliger 1992; Key et al. 1997; McClain et al. 1985).

To characterize atmospheric water vapor, PREFIRE will leverage complementary information in the MIR (~6 μm) and FIR water vapor bands. For similar instrument noise levels, the water vapor rotation bands in the FIR provide particularly strong signals at cold temperatures characteristic of polar regions and the upper troposphere enhancing accuracy in these conditions relative to MIR alone (Merrelli and Turner 2012; Coursol et al. 2020). However, retrievals will be susceptible to error due to semiempirical continuum absorption models that still have high uncertainty in the FIR (Mlawer et al. 2019). While the moderate spectral resolution of TIRS limits its ability to retrieval high-vertical-resolution temperature and water vapor profiles, the varying heights of TIRS weighting functions suggest that coarse vertical profiles can be retrieved provided reasonable prior constraints are supplied from meteorological analysis datasets.

In the colder, drier polar climates, the shorter wavelength portions of the FIR (15–25 μm) feature partially transmissive microwindows where some fraction of the surface leaving radiation reaches a space borne sensor [e.g., the 17-μm (blue) and 21-μm (purple) weighting functions in Fig. 8a]. With CWV and T_{sfc} constrained, the effects of the atmosphere on these channels can be modeled effectively "peeling back" the atmosphere to estimate surface emissivity in these microwindows. Since the surface emissivities of most surfaces vary slowly with wavelength (Fig. 3), the significant spectral features should be well sampled by the moderate spectral resolution of TIRS.

In cloudy profiles, TIRS radiances provide sensitivity to a wide range of polar cloud characteristics (Fig. 9). Spectral differences in the single scatter albedos of liquid and ice particles across the MIR and FIR (Rathke et al. 2002; Turner et al. 2003; Cox et al. 2010; Rowe et al. 2013; Maestri et al. 2019a,b; Di Natale et al. 2020) may offer improved cloud phase classification compared to MIR alone (Fig. 9b). Furthermore, supercooled water droplets have distinct scattering properties from those in warm clouds (above 0°C) enabling mixed-phase clouds to be identified (Turner 2005; Turner and Eloranta 2008).

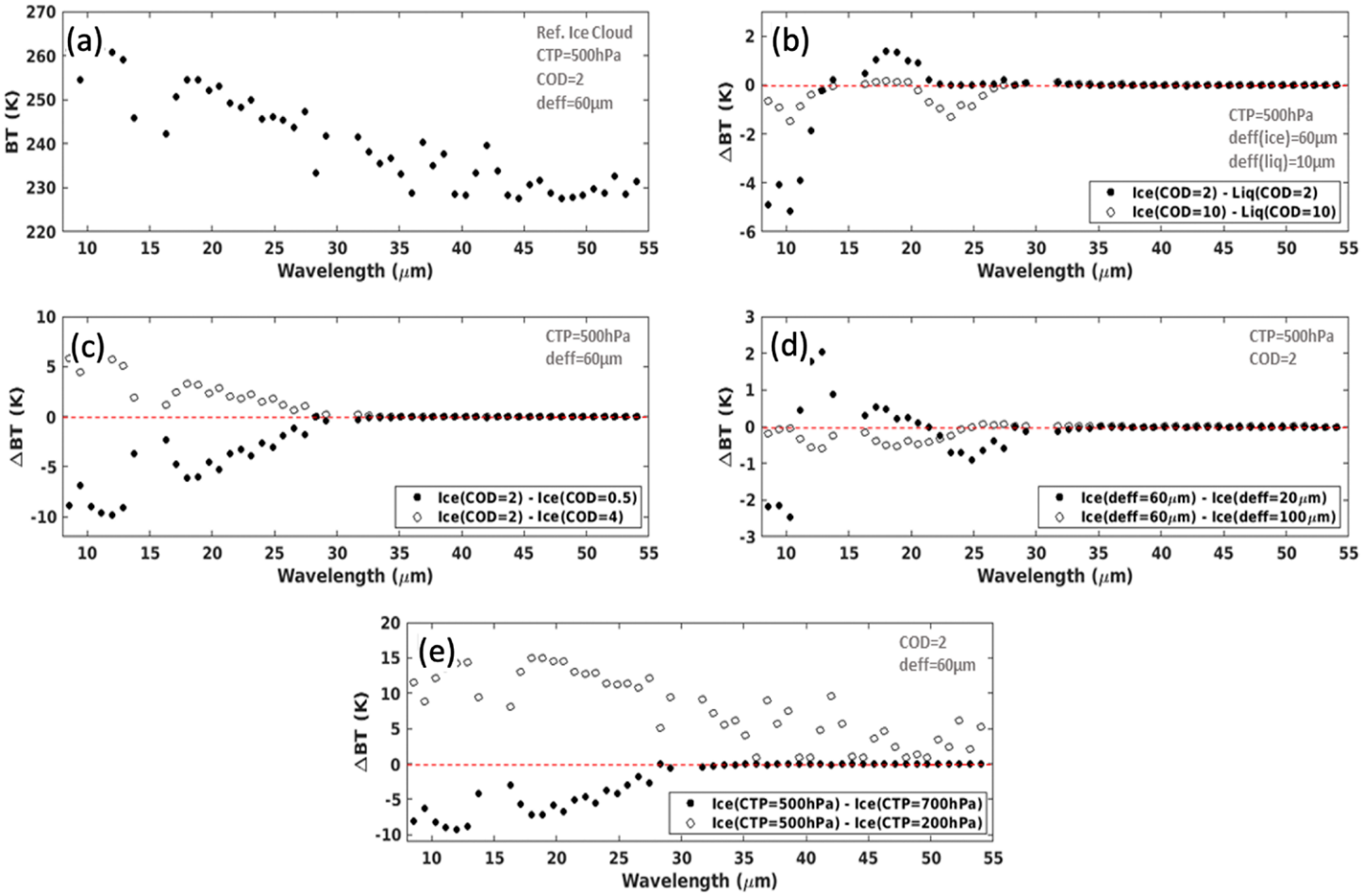

Fig. 9. (a) A simulated TIRS spectrum for an Arctic ice cloud with optical depth of 2 and effective diameter of 60 μm at 500 hPa. Ice crystal single scattering properties are consistent with the MODIS Collection 5 habit mixture (Yang et al. 2013; Baum et al. 2014). The remaining panels show brightness temperature differences relative to this cloud for (b) liquid clouds at the same height with effective diameters of 10 μm and optical depths of 2 and 5, (c) similar ice clouds with optical depths of 0.5 and 4, (d) ice clouds with effective diameters of 20 and 100 μm, and (e) ice clouds at 700 and 200 hPa. For all simulations, a typical Arctic January atmospheric profile is used.

The scattering properties of ice crystals also exhibit unique sensitivity to particle size in the far-infrared compared to the midinfrared (Baran 2007; Yang et al. 2013; Baum et al. 2014). This may substantially expand the dynamic range of ice particle size that can be retrieved with TIRS (Maestri et al. 2014; Maestri et al. 2019a,b; Libois and Blanchet 2017; Saito et al. 2020). However, computed scattering properties require ice crystal habit and size distribution assumptions that introduce uncertainty in relating radiances to particle size (Cooper et al. 2006). Prior efforts to evaluate bulk ice cloud scattering properties through the FIR using in situ observations are limited to select case studies (Cox et al. 2010; Bantges et al. 2020) so some refinement of existing particle optical properties may be required.

Benefit to polar modeling and prediction

PREFIRE's fundamental goal is to advance our understanding of polar climate. Its short lifetime, moderate spectral resolution, and modest radiometric accuracy precludes benchmarking polar climate trends but two CubeSats in distinct orbits, sampling the full spectrum of FIR emission over both poles for a year will characterize the spectral signatures of the atmospheric and surface processes that modulate local thermal emission across the dynamic polar annual cycle. These signatures provide a unique resource for both assessing and refining uncertain elements of ice sheet process models and GCMs.

PREFIRE observations offer two pathways for advancing polar climate and process models: directly refining surface emissivity models that influence surface–atmosphere energy exchange and assessing simulated spectral fluxes to identify potential biases in specific process models. The first requires interfacing PREFIRE products with ice sheet and climate models. Surface emissivity estimates spanning the range of polar environments will be aggregated into a new spectral surface emissivity database spanning both MIR and FIR wavelengths. With a straight-forward coupler that partitions broadband longwave fluxes into their spectral components, this database can be incorporated into models to replace assumed constant emissivities. Thus, PREFIRE's emissivity estimates offer the potential to immediately improve the modeling of surface emission that influences surface energy balance and associated surface processes.

The second pathway invokes the unique spectral signatures of specific surfaces and atmospheric constituents through the FIR to guide model improvement by providing insights into specific processes and modes of variability. Observed TIRS spectra and the AGHE estimates derived from them allow the contributions to OLR and DLR variability from changes in surface temperature, surface conditions, water vapor, and clouds to be isolated (Wielicki et al. 2013; Huang et al. 2014a). Comparing spectra derived from climate model inputs to PREFIRE observations may, therefore, reveal deficiencies in particular aspects of model physics. To encourage and facilitate credible comparisons throughout the global climate modeling community, a spectral radiance simulator that accounts for TIRS spatial resolution and sensitivity and associated diagnostics will be integrated into the Cloud Feedback Model Intercomparison Project (CFMIP) Observation Simulator Package (COSP) (Bodas-Salcedo et al. 2011). This simulator will enable "definition-aware" (i.e., defined based on TIRS instrument spectral resolution and radiometric accuracy) and "scale-aware" (i.e., at a consistent spatial scale) comparisons against monthly gridded, monthly spectral fluxes, AGHE, and cloud impacts on AGHE derived from PREFIRE all-sky and clear-sky spectra. Recent work has highlighted the value of instrument simulators in polar regions for both precipitation (Lenaerts et al. 2020) and clouds/atmospheric opacity (Morrison et al. 2019).

The influence of PREFIRE-inspired model improvements on predicted rates of Arctic warming, sea ice and ice sheet melt, and the associated global impacts will be assessed within the framework of long multicentury control runs and large initial condition ensembles (Kay et al. 2015; Deser et al. 2020). The joint influence of forced climate change and unforced variability on observed and projected polar ice loss and warming is often underappreciated. For example, Arctic sea ice cover can temporarily increase in a warming world (e.g., Kay et al. 2011) and the timing of an ice-free surface Arctic Ocean can vary by two decades due to internally generated unforced climate variability alone (Jahn et al. 2016). As a result, large initial-condition ensembles are required to fully document climate variability and change (Deser et al. 2020). Output from these large ensembles also provides initial conditions to drive ice sheet models to examine ice sheet surface energy balance, mass budget, and ice dynamic processes in a warming world. Sensitivity studies using the uncertainty quantification framework of the Ice-sheet and Sea level System Model (ISSM) and its Glacier and Energy Mass Balance (GEMB) module with PREFIRE-derived spectral surface emissivities and associated errors sorted according to surface type using ancillary products such as visible and microwave sea ice concentration will establish how internal variability and forced climate trends influence projected surface mass balance and ice sheet dynamic processes across the Greenland ice sheet (Fausto et al. 2016).

A new frontier in polar climate observations

The Polar Radiant Energy in the Far-Infrared Experiment builds upon decades of research revealing the importance of the far-infrared spectrum in Earth's energy balance and its value

for retrieving atmospheric properties to provide a new view of the planet through a far-infrared lens (e.g., Harries et al. 2008, and references therein). By extending current spectral infrared measurements into the FIR, PREFIRE will provide the most complete picture to date of the spectral character of Earth's emission opening a door to improved characterization of surface longwave radiative flux exchanges at the poles, better representation of spectral emissivity in process models and GCMs, and new diagnostics for evaluating the fingerprints of the processes that shape the polar climate.

PREFIRE is also among the first dedicated Earth science missions that will employ CubeSat technology for all of its measurements (Stephens et al. 2020). This affords the opportunity to fly two identical platforms in asynchronous polar orbits to directly identify the processes that influence longwave energy flows at both poles (see also Blackwell et al. 2018). Differences in observed spectra from time-lagged orbit intersections of these platforms quantify variations in surface emissivity owing to rapid surface processes (e.g., melting and freezing) and assess the drivers of AGHE (e.g., clouds and moisture gradients).

While PREFIRE primarily focuses on better characterizing polar far-infrared emission and the factors that modulate it, far-infrared spectra may also benefit several lower-latitude applications. The principles governing far-infrared radiances in polar regions apply in all cold, dry regions including high altitude mountain regions and the UTLS. FIR spectra may be particularly useful for characterizing spatial variations in UTLS temperature and water vapor associated with gravity waves and convection (Fueglistaler 2005; Nishimoto and Shiotani 2012; Schoeberl et al. 2015). Ferrare et al. (2004) show that the upper most 0.1 mm of water vapor in the atmospheric column must be constrained to within 10% to simulate clear-sky OLR to an accuracy of 0.5 W m^{-2} and water vapor at these altitudes has been shown to play a key role in defining global temperature trends (Dessler and Sherwood 2009; Solomon et al. 2010; Dessler 2013). However, water vapor variations in the lower stratosphere are currently poorly represented in global models (Hurst et al. 2011; Hegglin et al. 2014). Preliminary studies have demonstrated that assimilating FIR spectra can constrain upper tropospheric humidity in numerical weather prediction (NWP) models (Coursol et al. 2020). The TIRS simulator being developed for COSP provides the required observational operator to interface with forecast systems and PREFIRE's calibration and validation efforts will supply the required observational error covariances.

With the launches of PREFIRE, FORUM, and a proposed Canadian mission, the Thin Ice Clouds in the Far-Infrared Experiment (TICFIRE; Blanchet et al. 2011), the next 10 years promise to open an exciting new window into the Earth system by systematically documenting far-infrared spectra that account for up to half of the planetary emission. Together these missions offer the potential to establish a new frontier in Earth observation by providing up to a decade of sustained far-infrared measurements.

Acknowledgments. This work was supported by NASA under the Earth Ventures-Instrument (EV-I) program's Polar Radiant Energy in the Far-Infrared Experiment (PREFIRE) mission. Components of the work performed at the University of Wisconsin–Madison, University of Colorado Boulder, and University of Michigan were supported under the associated NASA PREFIRE Grant 80NSSC18K1485. Part of this research was carried out at the Jet Propulsion Laboratory (JPL), California Institute of Technology, under a contract with the National Aeronautics and Space Administration. We thank Helen Brindley, Jonathan Murray, and the TAFTS team for providing airborne observations of FIR spectra over Greenland.

Data availability statement. ARIES and TAFTS data were acquired through the Met Office (2016).

References

Ackerman, S. A., K. I. Strabala, W. P. Menzel, R. A. Frey, C. C. Moeller, and L. E. Gumley, 1998: Discriminating clear sky from clouds with MODIS. *J. Geophys. Res.*, **103**, 32 141–32 157, https://doi.org/10.1029/1998JD200032.

——, and Coauthors, 2019: Satellites see the world's atmosphere. *A Century of Progress in Atmospheric and Related Sciences: Celebrating the American Meteorological Society Centennial*, *Meteor. Monogr.*, No. 59, Amer. Meteor. Soc., https://doi.org/10.1175/AMSMONOGRAPHS-D-18-0009.1.

Bantges, R. J., and Coauthors, 2020: A test of the ability of current bulk optical models to represent the radiative properties of cirrus cloud across the mid- and far-infrared. *Atmos. Chem. Phys.*, **20**, 12 889–12 903, https://doi.org/10.5194/acp-20-12889-2020.

Baran, A. J., 2007: The impact of cirrus microphysical and macrophysical properties on upwelling far-infrared spectra. *Quart. J. Roy. Meteor. Soc.*, **133**, 1425–1437, https://doi.org/10.1002/qj.132.

Baum, B. A., P. Yang, A. J. Heymsfield, A. Bansemer, A. Merrelli, C. Schmitt, and C. Wang, 2014: Ice cloud bulk single-scattering property models with the full phase matrix at wavelengths from 0.2 to 100 μm. *J. Quant. Spectrosc. Radiat. Transfer*, **146**, 123–139, https://doi.org/10.1016/j.jqsrt.2014.02.029.

Bellisario, C., and Coauthors, 2017: Retrievals of the far infrared surface emissivity over the Greenland Plateau using the Tropospheric Airborne Fourier Transform Spectrometer (TAFTS). *J. Geophys. Res.*, **122**, 12 152–12 166, https://doi.org/10.1002/2017JD027328.

Bennartz, R., and Coauthors, 2013: July 2012 Greenland melt extent enhanced by low-level liquid clouds. *Nature*, **496**, 83–86, https://doi.org/10.1038/nature12002.

Blackwell, W. J., and Coauthors, 2018: An overview of the TROPICS NASA Earth Venture Mission. *Quart. J. Roy. Meteor. Soc.*, **144**, 16–26, https://doi.org/10.1002/qj.3290.

Blanchet, J.-P., and Coauthors, 2011: TICFIRE: A far infrared payload to monitor the evolution of thin ice clouds. *Proc. SPIE*, **8176**, 81761K, https://doi.org/10.1117/12.898577.

Bodas-Salcedo, A., and Coauthors, 2011: COSP: Satellite simulation software for model assessment. *Bull. Amer. Meteor. Soc.*, **92**, 1023–1043, https://doi.org/10.1175/2011BAMS2856.1.

Budyko, M. I., 1969: The effect of solar radiation variations on the climate of the Earth. *Tellus*, **21**, 611–619, https://doi.org/10.3402/tellusa.v21i5.10109.

Chen, X. H., X. L. Huang, N. G. Loeb, and H. L. Wei, 2013: Comparisons of clear-sky outgoing far-IR flux inferred from satellite observations and computed from three most recent reanalysis products. *J. Climate*, **26**, 478–494, https://doi.org/10.1175/JCLI-D-12-00212.1.

Chen, Y.-H., 2020: Influences of surface spectral emissivity and cloud longwave scattering on climate simulations. Ph.D. thesis, University of Michigan at Ann Arbor, 160 pp.

Clough, S. A., M. J. Iacono, and J.-L. Moncet, 1992: Line-by-line calculations of atmospheric fluxes and cooling rates: Application to water vapor. *J. Geophys. Res.*, **97**, 15 761–15 785, https://doi.org/10.1029/92JD01419.

Conrath, B. J., R. A. Hanel, V. G. Kunde, and C. Prabhakara, 1970: The Infrared Interferometer Experiment on Nimbus 3. *J. Geophys. Res.*, **75**, 5831–5857, https://doi.org/10.1029/JC075i030p05831.

Cooper, S. J., T. S. L'Ecuyer, P. Gabriel, G. L. Stephens, A. J. Baran, and P. Yang, 2006: Objective assessment of the information content of visible and infrared radiance measurements for cloud microphysical property retrievals over the global oceans. Part II: Ice clouds. *J. Appl. Meteor.*, **45**, 42–62, https://doi.org/10.1175/JAM2327.1.

Coursol, L., Q. Libois, P. Gauthier, and J.-P. Blanchet, 2020: Optimal configuration of a far-infrared radiometer to study the Arctic winter atmosphere. *J. Geophys. Res. Atmos.*, **125**, e2019JD031773, https://doi.org/10.1029/2019JD031773.

Cox, C. V., J. E. Harries, J. P. Taylor, P. D. Green, A. J. Baran, J. C. Pickering, A. E. Last, and J. E. Murray, 2010: Measurement and simulation of mid- and far-infrared spectra in the presence of cirrus. *Quart. J. Roy. Meteor. Soc.*, **136**, 718–739, https://doi.org/10.1002/qj.596.

Deser, C., and Coauthors, 2020: Insights from Earth system model initial-condition large ensembles and future prospects. *Nat. Climate Change*, **10**, 277–286, https://doi.org/10.1038/s41558-020-0731-2.

Dessler, A. E., 2013: Observations of climate feedbacks over 2000–10 and comparisons to climate models. *J. Climate*, **26**, 333–342, https://doi.org/10.1175/JCLI-D-11-00640.1.

——, and S. C. Sherwood, 2009: A matter of humidity. *Science*, **323**, 1020–1021, https://doi.org/10.1126/science.1171264.

Di Natale, G., G. Bianchini, M. Del Guasta, M. Ridolfi, T. Maestri, W. Cossich, D. Magurno, and L. Palchetti, 2020: Characterization of the far-infrared properties and radiative forcing of Antarctic ice and water clouds exploiting the spectrometer-lidar synergy. *Remote Sens.*, **12**, 3574–3595, https://doi.org/10.3390/rs12213574.

Fausto, R. S., D. van As, J. E. Box, W. Colgan, and P. L. Langen, 2016: Quantifying the surface energy fluxes in south Greenland during the 2012 high melt episodes using *in situ* observations. *Front. Earth Sci.*, **4**, 82, https://doi.org/10.3389/feart.2016.00082.

Ferrare, R. A., and Coauthors, 2004: Characterization of upper-troposphere water vapor measurements during AFWEX using LASE. *J. Atmos. Oceanic Technol.*, **21**, 1790–1808, https://doi.org/10.1175/JTECH-1652.1.

Francis, J. A., and S. J. Vavrus, 2012: Evidence linking Arctic amplification to extreme weather in mid-latitudes. *Geophys. Res. Lett.*, **39**, L06801, https://doi.org/10.1029/2012GL051000.

——, E. Hunter, J. R. Key, and X. Wang, 2005: Clues to variability in Arctic minimum sea ice extent. *Geophys. Res. Lett.*, **32**, L21501, https://doi.org/10.1029/2005GL024376.

Fueglistaler, S., 2005: Stratospheric water vapor predicted from the Lagrangian temperature history of air entering the stratosphere in the tropics. *J. Geophys. Res.*, **110**, D08107, https://doi.org/10.1029/2004JD005516.

Gardner, A. S., 2010: Surface mass balance of Arctic glaciers: Climate influences and modeling approaches. Ph.D. dissertation, University of Alberta, 195 pp., https://doi.org/10.7939/R3FB4WX73.

Hanel, R. A., B. Schlachman, F. D. Clark, C. H. Prokesh, J. B. Taylor, W. M. Wilson, and L. Chaney, 1970: The Nimbus III Michelson interferometer. *Appl. Opt.*, **9**, 1767–1774, https://doi.org/10.1364/AO.9.001767.

——, ——, D. Rogers, and D. Vanous, 1971: Nimbus 4 Michelson interferometer. *Appl. Opt.*, **10**, 1376–1382, https://doi.org/10.1364/AO.10.001376.

Harries, J. E., and Coauthors, 2008: The far-infrared Earth. *Rev. Geophys.*, **46**, RG4004, https://doi.org/10.1029/2007RG000233.

Hegglin, M. I., and Coauthors, 2014: Vertical structure of stratospheric water vapour trends derived from merged satellite data. *Nat. Geosci.*, **7**, 768–776, https://doi.org/10.1038/ngeo2236.

Heidinger, A. K., and M. J. Pavolonis, 2009: Gazing at cirrus clouds for 25 years through a split window. Part I: Methodology. *J. Appl. Meteor. Climatol.*, **48**, 1100–1116, https://doi.org/10.1175/2008JAMC1882.1.

Henderson, D. S., T. L'Ecuyer, G. Stephens, P. Partain, and M. Sekiguchi, 2013: A multisensor perspective on the radiative impacts of clouds and aerosols. *J. Appl. Meteor. Climatol.*, **52**, 853–871, https://doi.org/10.1175/JAMC-D-12-025.1.

Huang, X. L., W. Z. Yang, N. G. Loeb, and V. Ramaswamy, 2008: Spectrally resolved fluxes derived from collocated AIRS and CERES measurements and their application in model evaluation: 1. Clear sky over the tropical oceans. *J. Geophys. Res.*, **113**, D09110, https://doi.org/10.1029/2007JD009219.

——, N. G. Loeb, and W. Z. Yang, 2010: Spectrally resolved fluxes derived from collocated AIRS and CERES measurements and their application in model evaluation: 2. Cloudy sky and band-by-band cloud radiative forcing over the tropical oceans. *J. Geophys. Res.*, **115**, D21101, https://doi.org/10.1029/2010JD013932.

——, X. H. Chen, B. J. Soden, and X. Liu, 2014a: The spectral dimension of longwave feedbacks in the CMIP3 and CMIP5 experiments. *Geophys. Res. Lett.*, **41**, 7830–7837, https://doi.org/10.1002/2014GL061938.

——, ——, G. L. Potter, L. Oreopoulos, J. N. S. Cole, D. M. Lee, and N. G. Loeb, 2014b: A global climatology of outgoing longwave spectral cloud radiative effect and associated effective cloud properties. *J. Climate*, **27**, 7475–7492, https://doi.org/10.1175/JCLI-D-13-00663.1.

——, ——, D. K. Zhou, and X. Liu, 2016: An observationally based global band-by-band surface emissivity dataset for climate and weather simulations. *J. Atmos. Sci.*, **73**, 3541–3555, https://doi.org/10.1175/JAS-D-15-0355.1.

——, ——, M. G. Flanner, P. Yang, D. Feldman, and C. Kuo, 2018: Improved representation of surface spectral emissivity in a global climate model and its impact on simulated climate. *J. Climate*, **31**, 3711–3727, https://doi.org/10.1175/JCLI-D-17-0125.1.

——, ——, and Q. Yue, 2019: Band-by-band contributions to the longwave cloud radiative feedbacks. *Geophys. Res. Lett.*, **46**, 6998–7006, https://doi.org/10.1029/2019GL083466.

Hulley, G. C., S. J. Hook, E. Manning, S.-Y. Lee, and E. Fetzer, 2009: Validation of the Atmospheric Infrared Sounder (AIRS) version 5 land surface emissivity product over the Namib and Kalahari Deserts. *J. Geophys. Res.*, **114**, D19104, https://doi.org/10.1029/2009JD012351.

Hurst, D. F., S. J. Oltmans, H. Vömel, K. H. Rosenlof, S. M. Davis, E. A. Ray, E. G. Hall, and A. F. Jordan, 2011: Stratospheric water vapor trends over Boulder, Colorado: Analysis of the 30-year Boulder record. *J. Geophys. Res.*, **116**, D02306, https://doi.org/10.1029/2010JD015065.

Inoue, T., 1985: On the temperature and effective emissivity determination of semi-transparent cirrus clouds by bispectral measurements in the 10 micron window region. *J. Meteor. Soc. Japan*, **63**, 88–99, https://doi.org/10.2151/jmsj1965.63.1_88.

Jahn, A., J. E. Kay, M. M. Holland, and D. M. Hall, 2016: How predictable is the timing of a summer ice-free Arctic? *Geophys. Res. Lett.*, **43**, 9113–9120, https://doi.org/10.1002/2016GL070067.

Johansson, E., A. Devasthale, M. Tjernstrom, A. M. L. Ekman, and T. L'Ecuyer, 2017: Response of the lower troposphere to moisture intrusions into the Arctic. *Geophys. Res. Lett.*, **44**, 2527–2536, https://doi.org/10.1002/2017GL072687.

Kahn, B. H., and Coauthors, 2014: The Atmospheric Infrared Sounder version 6 cloud products. *Atmos. Chem. Phys.*, **14**, 399–426, https://doi.org/10.5194/acp-14-399-2014.

——, B. J. Drouin, and T. S. L'Ecuyer, 2020: Evaluation of AIRS assessment of sampling sufficiency for low-cost satellite missions: Application to PREFIRE. *J. Atmos. Oceanic Technol.*, **37**, 2283–2298, https://doi.org/10.1175/JTECH-D-20-0023.1.

Kapsch, M.-L., R. G. Graverson, M. Tjernstrom, and R. Bintanja, 2016: The effect of downwelling longwave and shortwave radiation on Arctic summer sea ice. *J. Climate*, **29**, 1143–1159, https://doi.org/10.1175/JCLI-D-15-0238.1.

Kay, J. E., M. M. Holland, and A. Jahn, 2011: Inter-annual to multi-decadal Arctic sea ice extent trends in a warming world. *Geophys. Res. Lett.*, **38**, L15708, https://doi.org/10.1029/2011GL048008.

——, and Coauthors, 2015: The Community Earth System Model (CESM) large ensemble project: A community resource for studying climate change in the presence of internal climate variability. *Bull. Amer. Meteor. Soc.*, **96**, 1333–1349, https://doi.org/10.1175/BAMS-D-13-00255.1.

Key, J., and M. Haefliger, 1992: Arctic ice surface temperature retrieval from AVHRR thermal channels. *J. Geophys. Res.*, **97**, 5885–5893, https://doi.org/10.1029/92JD00348.

——, J. B. Collins, C. Fowler, and R. S. Stone, 1997: High-latitude surface temperature estimates from thermal satellite data. *Remote Sens. Environ.*, **61**, 302–309, https://doi.org/10.1016/S0034-4257(97)89497-7.

Kuo, C., D. R. Feldman, X. Huang, M. Flanner, P. Yang, and X. Chen, 2018: Time-dependent cryospheric longwave surface emissivity feedback in the Community Earth System Model. *J. Geophys. Res. Atmos.*, **123**, 789–813, https://doi.org/10.1002/2017JD027595.

L'Ecuyer, T. S., and Coauthors, 2015: The observed state of global energy balance in the early 21st century. *J. Climate*, **28**, 8319–8346, https://doi.org/10.1175/JCLI-D-14-00556.1.

Lenaerts, J., M. D. Camron, C. Wyburn-Powell, and J. E. Kay, 2020: Present-day and future Greenland ice sheet precipitation frequency from satellite observations and an Earth system model. *Cryosphere*, **14**, 2253–2265, https://doi.org/10.5194/tc-14-2253-2020.

Libois, Q., and J.-P. Blanchet, 2017: Added value of far-infrared radiometry for remote sensing of ice clouds. *J. Geophys. Res. Atmos.*, **122**, 6541–6564, https://doi.org/10.1002/2016JD026423.

Maestri, T., and R. Rizzi, 2003: A study of infrared diabatic forcing of ice clouds in the tropical atmosphere. *J. Geophys. Res.*, **108**, 4139, https://doi.org/10.1029/2002JD002146.

——, and Coauthors, 2014: Analysis of cirrus cloud spectral signatures in the far infrared. *J. Quant. Spectrosc. Radiat. Transfer*, **141**, 49–64, https://doi.org/10.1016/j.jqsrt.2014.02.030.

——, C. Arosio, R. Rizzi, L. Palchetti, G. Bianchini, and M. Del Guasta, 2019a: Antarctic ice cloud identification and properties using downwelling spectral radiance from 100 to 1,400 cm^{-1}. *J. Geophys. Res.*, **124**, 4761–4781, https://doi.org/10.1029/2018JD029205.

——, W. Cossich, and I. Sbrolli, 2019b: Cloud identification and classification from high spectral resolution data in the far infrared and mid-infrared. *Atmos. Meas. Tech.*, **12**, 3521–3540, https://doi.org/10.5194/amt-12-3521-2019.

McClain, E. P., W. G. Pichel, and C. C. Walton, 1985: Comparative performance of AVHRR-based multichannel sea surface temperatures. *J. Geophys. Res.*, **90**, 11 587–11 601, https://doi.org/10.1029/JC090iC06p11587.

Menzel, W. P., and Coauthors, 2008: MODIS global cloud-top pressure and amount estimation: Algorithm description and results. *J. Appl. Meteor. Climatol.*, **47**, 1175–1198, https://doi.org/10.1175/2007JAMC1705.1.

Merrelli, A., and D. D. Turner, 2012: Comparing information content of upwelling far-infrared and midinfrared radiance spectra for clear atmosphere profiling. *J. Atmos. Oceanic Technol.*, **29**, 510–526, https://doi.org/10.1175/JTECH-D-11-00113.1.

Met Office, 2016: FAAM B898 COSMICS flight: Airborne atmospheric measurements from core and non-core instrument suites on board the BAE-146 aircraft. NCAS British Atmospheric Data Centre, accessed 12 November 2020, https://catalogue.ceda.ac.uk/uuid/b5758a268bf74497b658628e8b4d7199.

Mlawer, E. J., and Coauthors, 2019: Analysis of water vapor absorption in the far-infrared and submillimeter regions using surface radiometric measurements from extremely dry locations. *J. Geophys. Res. Atmos.*, **124**, 8134–8160, https://doi.org/10.1029/2018JD029508.

Morrison, A. L., J. E. Kay, W. R. Frey, H. Chepfer, and R. Guzman, 2019: Cloud response to Arctic sea ice loss and implications for future feedbacks in the CESM1 climate model. *J. Geophys. Res. Atmos.*, **124**, 1003–1020, https://doi.org/10.1029/2018JD029142.

Murray, J. E., and Coauthors, 2020: Retrievals of high-latitude surface emissivity across the infrared from high altitude aircraft flights. *J. Geophys. Res.*, **125**, e2020JD033672, https://doi.org/10.1029/2020JD033672.

Nishimoto, E., and M. Shiotani, 2012: Seasonal and interannual variability in the temperature structure around the tropical tropopause and its relationship with convective activities. *J. Geophys. Res.*, **117**, D02104, https://doi.org/10.1029/2011JD016936.

Palchetti, L., G. Bianchini, G. Di Natale, and M. Del Guasta, 2015: Far-infrared radiative properties of water vapor and clouds in Antarctica. *Bull. Amer. Meteor. Soc.*, **96**, 1505–1518, https://doi.org/10.1175/BAMS-D-13-00286.1.

——, and Coauthors, 2020: FORUM: Unique far-infrared satellite observations to better understand how Earth radiates energy to space. *Bull. Amer. Meteor. Soc.*, **101**, E2030–E2046, https://doi.org/10.1175/BAMS-D-19-0322.1.

Pan, F., and X. L. Huang, 2018: The spectral dimension of modeled relative humidity feedbacks in the CMIP5 experiments. *J. Climate*, **31**, 10 021–10 038, https://doi.org/10.1175/JCLI-D-17-0491.1.

Prabhakara, C., G. Dalu, and V. G. Kunde, 1974: A search for global and seasonal variation of methane from Nimbus 4 IRIS measurements. *J. Geophys. Res.*, **79**, 1744–1749, https://doi.org/10.1029/JC079i012p01744.

——, E. B. Rodgers, B. J. Conrath, R. A. Hanel, and V. G. Kunde 1976: The Nimbus 4 infrared spectroscopy experiment: 3. Observations of the lower stratospheric

thermal structure and total ozone. *J. Geophys. Res.*, **81**, 6391–6399, https://doi.org/10.1029/JC081i036p06391.

——, R. S. Fraser, G. Dalu, M.-L. C. Wu, R. J. Curran, and T. Styles, 1988: Thin cirrus clouds: Seasonal distribution over oceans deduced from *Nimbus-4* IRIS. *J. Appl. Meteor.*, **27**, 379–399, https://doi.org/10.1175/1520-0450(1988)027<0379:TCCSDO>2.0.CO;2.

Rathke, C., J. Fishcer, S. Neshyba, and M. Shupe, 2002: Improving IR cloud phase determination with 20 micrometers spectral observations. *Geophys. Res. Lett.*, **29**, 1209, https://doi.org/10.1029/2001GL014594.

Rossow, W. B., and R. A. Schiffer, 1991: ISCCP cloud data products. *Bull. Amer. Meteor. Soc.*, **72**, 2–20, https://doi.org/10.1175/1520-0477(1991)0722.0.CO;2.

Rowe, P. M., S. Neshyba, and V. P. Walden, 2013: Radiative consequences of low-temperature infrared refractive indices for super-cooled water clouds. *Atmos. Chem. Phys.*, **13**, 11 925–11 933, https://doi.org/10.5194/acp-13-11925-2013.

Saito, M., P. Yang, X. Huang, H. E. Brindley, M. G. Mlynczak, and B. H. Kahn, 2020: Spaceborne middle- and far-infrared observations improving nighttime ice cloud property retrievals. *Geophys. Res. Lett.*, **47**, e2020GL087491, https://doi.org/10.1029/2020GL087491.

Schoeberl, M. R., E. J. Jensen, and S. Woods, 2015: Gravity waves amplify upper tropospheric dehydration by clouds. *Earth Space Sci.*, **2**, 485–500, https://doi.org/10.1002/2015EA000127.

Schweiger, A. J., J. Zhang, R. W. Lindsay, and M. Steele, 2008: Did unusually sunny skies help drive the record sea ice minimum of 2007? *Geophys. Res. Lett.*, **35**, L10503, https://doi.org/10.1029/2008GL033463.

Shahabadi, M. B., and Y. Huang, 2014: Measuring stratospheric H_2O with an airborne spectrometer. *J. Atmos. Oceanic Technol.*, **31**, 1502–1515, https://doi.org/10.1175/JTECH-D-13-00191.1.

Slater, T., A. E. Hogg, and R. Mottram, 2020: Ice-sheet losses track high-end sea-level rise projections. *Nat. Climate Change*, **10**, 879–881, https://doi.org/10.1038/s41558-020-0893-y.

Sledd, A., and T. L'Ecuyer, 2019: How much do clouds mask the impact of Arctic sea ice and snow cover variations? Different perspectives from observations and reanalyses. *Atmosphere*, **10**, 12, https://doi.org/10.3390/atmos10010012.

Solomon, S., K. H. Rosenlof, R. W. Portmann, J. S. Daniel, S. M. Davis, T. J. Sanford, and G.-K. Plattner, 2010: Contributions of stratospheric water vapor to decadal changes in the rate of global warming. *Science*, **327**, 1219–1223, https://doi.org/10.1126/science.1182488.

Spankuch, D., and W. Dohler, 1985: Radiative properties of cirrus clouds in the middle IR derived from Fourier spectrometer measurements from space. *Z. Meteor.*, **35**, 314–324.

Stephens, G. L., and Coauthors, 2020: The emerging technological revolution in Earth observations. *Bull. Amer. Meteor. Soc.*, **101**, E274–E285, https://doi.org/10.1175/BAMS-D-19-0146.1.

Turner, D. D., 2005: Arctic mixed-phase cloud properties from AERI lidar observations: Algorithm and results from SHEBA. *J. Appl. Meteor.*, **44**, 427–444, https://doi.org/10.1175/JAM2208.1.

——, and E. W. Eloranta, 2008: Validating mixed-phase cloud optical depth retrieved from infrared observations with high spectral resolution lidar. *IEEE Geosci. Remote Sens. Lett.*, **5**, 285–288, https://doi.org/10.1109/LGRS.2008.915940.

——, and E. J. Mlawer, 2010: Radiative Heating in Underexplored Bands Campaigns (RHUBC). *Bull. Amer. Meteor. Soc.*, **91**, 911–924, https://doi.org/10.1175/2010BAMS2904.1.

——, S. A. Ackerman, B. A. Baum, H. E. Revercomb, and P. Yang, 2003: Cloud phase determination using ground-based AERI observations at SHEBA. *J. Appl. Meteor.*, **42**, 701–715, https://doi.org/10.1175/1520-0450(2003)0422.0.CO;2.

——, A. Merrelli, D. Vimont, and E. J. Mlawer, 2012: Impact of modifying the longwave water vapor continuum absorption model on Community Earth System Model simulations. *J. Geophys. Res.*, **117**, D04106, https://doi.org/10.1029/2011JD016440.

Van Tricht, K., and Coauthors, 2016: Clouds enhance Greenland ice sheet meltwater runoff. *Nat. Commun.*, **7**, 10266, https://doi.org/10.1038/ncomms10266.

Vihma, T., 2014: Effects of Arctic sea ice decline on weather and climate: A review. *Surv. Geophys.*, **35**, 1175–1214, https://doi.org/10.1007/s10712-014-9284-0.

Wielicki, B. A., and Coauthors, 2013: Achieving climate change absolute accuracy in orbit. *Bull. Amer. Meteor. Soc.*, **94**, 1519–1539, https://doi.org/10.1175/BAMS-D-12-00149.1.

Yang, P., and Coauthors, 2003: Spectral signature of ice clouds in the far-infrared region: Single-scattering calculations and radiative sensitivity study. *J. Geophys. Res.*, **108**, 4569, https://doi.org/10.1029/2002JD003291.

——, H. Wei, H.-L. Huang, B. A. Baum, Y. X. Hu, G. W. Kattawar, M. I. Mishchenko, and Q. Fu, 2005: Scattering and absorption property database for nonspherical ice particles in the near- through far-infrared spectral region. *Appl. Opt.*, **44**, 5512–5523, https://doi.org/10.1364/AO.44.005512.

——, L. Bi, B. A. Baum, K. N. Liou, G. W. Kattawar, and M. Mishchenko, 2013: Spectrally consistent scattering, absorption, and polarization properties of atmospheric ice crystals at wavelengths from 0.2 to 100 μm. *J. Atmos. Sci.*, **70**, 330–347, https://doi.org/10.1175/JAS-D-12-039.1.

Zhou, L., and Coauthors, 2008: Regression of surface spectral emissivity from hyperspectral instruments. *IEEE Trans. Geosci. Remote Sens.*, **46**, 328–333, https://doi.org/10.1109/TGRS.2007.912712.